Hollow polymer-silica particles as an alternative to TiO2 opacifiers

Constantina Sofroniou, Sarah Chong, Timothy Murdoch, Edgar Espinosa Rodriguez, Franck D'Agosto, Muriel Lansalot, Stefano Sacanna, Ignacio Martín-Fabiani

Hollow polymer-silica particles as an alternative to TiO_2 opacifiers

Constantina Sofroniou[1]*, *Sarah Chong*[2], *Timothy J. Murdoch*[1], *Edgar Espinosa Rodriguez*[3], *Franck D'Agosto*[3], *Muriel Lansalot*[3], *Stefano Sacanna*[2], *Ignacio Martín-Fabiani*[1]

1 Department of Materials, Loughborough University, LE11 3TU Loughborough, UK.

2 Department of Chemistry, New York University, NY 10003-6688 New York, USA.

3 Universite Claude Bernard Lyon 1, CPE Lyon, CNRS, UMR 5128, Catalysis, Polymerization, Processes and Materials (CP2M), Villeurbanne F-69616, France.

*corresponding author: Constantina Sofroniou, c.sofroniou@lboro.ac.uk

KEYWORDS: Coatings, Opacifiers, Hollow particles, Reflectance

ABSTRACT

The significant environmental impact associated with TiO_2 production has prompted the exploration of more sustainable alternatives for opacifiers. Polymeric hollow particles (HPs)

emerged as promising candidates, but they have not yet been able to fully replace TiO_2 in coatings. In this study, we report for the first time a total replacement of TiO_2 using polymer-silica HPs, achieving comparable or superior optical properties. We investigate 3-(trimethoxysilyl)propyl methacrylate (TPM) HPs with different size and shell thickness in coatings formed under different environmental conditions in the presence of polymeric binder particles. The smaller HPs (1 μm diameter, 0.2 μm shell thickness) demonstrated superior optical properties, achieving solar reflectance values up to 73.3% across the visible and near infrared spectrum. They outperformed both larger HPs (~5 μm diameter, 0.25 μm shell thickness) and TiO_2 reference coatings containing the same mass percentage of opacifier. We report various film microstructures depending on the film forming conditions and correlate them with the interplay between diffusion, evaporation, and sedimentation processes. Importantly, high optical performance was maintained across the range of microstructures found, indicating reduced sensitivity to HP distribution within the coating. This is a promising feature when it comes to reliability of use in a range of industrial formulations.

1. INTRODUCTION

Opacifiers are incorporated to reduce light transmission and create a visual barrier by masking or hiding the underlying surface. They play a crucial role in various applications where complete coverage is essential, including paints[1,2], food,[3] cosmetics,[4] inks,[5] pharmaceuticals,[6] and many others. While the primary function of opacifiers is to mask the underlying substrate in a uniform way for aesthetic reasons, they usually also impart protective and functional characteristics to the coating.[7–9]

Metal oxides dominate the opacifiers market. Titanium dioxide (TiO_2) is the most popular because of its exceptional light-scattering properties.[10] TiO_2 global demand is expected to reach around 8 million tonnes by 2025, with paints and coatings taking the largest share (around 55%).[11] However, the production of TiO_2 comes with significant environmental burden, primarily associated with manufacturing processes with large carbon footprint, producing 550 kg of CO_2 per ton of TiO_2.[12,13] Additionally, TiO_2 and other metal oxides often demonstrate limited colloidal stability, and are prone to aggregation or degradation under various environmental conditions.[14,15] These challenges can not only affect the long-term optical performance of coatings but also increase production and formulation costs due to the need for surface treatments, stabilizers, and strict processing conditions.

In the search for a more sustainable alternative to TiO_2, polymeric hollow particles (HPs) have been proposed as a potential low-impact replacement.[16] HPs consist of a hollow core surrounded by a polymeric shell. The core is filled with water when in dispersion and later replaced by air upon drying. This particle morphology enhances refractive index contrast and can effectively block light transmission, achieving high opacity at low solid contents.[17,18] The light-scattering mechanism of HPs involves multiple internal reflections and enhanced scattering phenomena.[19,20] This has been nicely demonstrated in studies comparing solid

versus hollow SiO_2 or TiO_2 particles.[21,22] Polymeric hollow particles were first patented by the Dow Chemical Company in 1984.[23] A commercial product based on them, ROPAQUE™, was released in the same year and can still be found in the market in different grades. However, ROPAQUE™ only allows for partial replacement of TiO_2, generally not above 30 wt.%,[24] and a full replacement has not been reported to date. Another advantage of polymeric HPs is their broader spectral reflectance when compared with TiO_2. It covers the Vis-NIR region, whereas TiO_2 is primarily limited to the UV-Vis range.[25] HPs can both enhance opacity and reduce heat absorption by reflecting a significant portion of incident solar radiation, thereby lowering cooling demands in buildings.[26,27] Additionally, the ability to tailor the surface chemistry of HPs, incorporate steric stabilization, and introduce functional groups can provide new opportunities for stimuli-responsive materials while enhancing their stability and dispersibility with the matrix they are embedded in.[28–30]

Here, we investigate the use of hybrid polymer-silica HPs synthesised from 3-(trimethoxysilyl)propyl methacrylate (TPM)[31] as opacifiers. The synthesis of HPs proceeds under mild, aqueous conditions at ambient temperature, in contrast to the high-temperature calcination or acid-based processing typically required in TiO_2 production.[32–34] This process has the potential to reduce energy consumption, which could be translated into lower manufacturing costs. We incorporate negatively charged TPM HPs with two different morphologies into coatings formulations alongside film-forming polymer particles with either positive or negative surface charges. The two HP architectures differ in both overall size and shell thickness: HP1 has a diameter of 5 μm and a 0.25 μm shell, while HP2 has a diameter of 1 μm and a 0.2 μm shell. The optical properties of the resulting coatings are evaluated and compared with control TiO_2-containing coatings to assess the potential of HPs as alternative opacifiers. We investigate how environmental conditions like relative humidity during film formation impact HP distribution and coating microstructure. These structural observations are

analyzed in the context of diffusion, evaporation, and sedimentation dynamics. To the best of our knowledge, this is the first report demonstrating a complete replacement of TiO_2 nanoparticles by hollow polymer-based particles in coatings formulations resulting in comparable or superior optical performance.

2. EXPERIMENTAL SECTION

2.1 Materials and Synthesis Methods.

Titanium (IV) oxide Aeroxide P25 in white powder form (TiO_2, Fisher Scientific) was used as received. H_2O used in this work was Milli-Q water (18.2 MΩ cm^{-1}, Synergy® UV). The synthesis of binder particles (synthesis of PDMAPMA and PSSNa macromolecular RAFT (macroRAFT) agents and the emulsion copolymerization of n-butyl acrylate and methyl methacrylate) is described in the Supporting Information. For the synthesis of hollow particles, the following chemicals were used: ammonia solution (28% Sigma-Aldrich), 3-(trimethoxysilyl)propyl methacrylate (TPM) (98%, Sigma-Aldrich), NaOH (>97%, Sigma-Aldrich), photoinitiator (Darocur 1173, Sigma-Aldrich).

Synthesis of hollow particles. A 300 mL glass beaker was placed on a Corning PC-420D stir plate, and 250 mL of deionized (DI) water was added. The solution was stirred continuously at 650 rpm. Then, 250 μL of 28% ammonia solution was added, and the beaker was immediately covered to minimize evaporation. The ammonia was allowed to mix for one minute before adding 1 mL of TPM. This mixture was stirred for 30 minutes at room temperature.

In a separate 750 mL Pyrex glass bottle, 400 mL of 133 mM NaOH solution and 300 μL of photoinitiator were combined and shaken thoroughly for another minute. Then 133 mL of the TPM emulsion solution was rapidly added to this NaOH solution to start the self-inflation process where the OH groups degrade the oil droplets, leading to an internal osmotic pressure buildup to form the inner cavities as described by Xu et.al.[31] At this stage, ammonia catalyzes the hydrolysis and condensation of the trimethoxy silyl groups of TPM, generating Si-O-Si linkages and silica-like domains in the forming shell. The bottle was immediately capped and overturned twice before inserting it into a UV lamp reactor for 30 minutes. Upon UV irradiation, the methacrylate groups polymerize, resulting in a cross-linked network interpenetrated with inorganic domains. Once polymerized, the particles were washed into DI

water through five centrifugation cycles, each time removing the supernatant and resuspending the sediment in DI water. This was done to ensure removal of unreacted chemicals and for long term colloidally stable storage. The resulting hollow particles (referred to as HP2 in this study) were of 1.0 μm diameter. To synthesize the larger HPs with 5.0 μm diameter (HP1), 8 mL of TPM was added to 72 mL of DI water and allowed to hydrolyze for 2 hours until the mixture was clear. To a 50 mL tube, 16 mL of DI and 5 μL of diluted 6% ammonia were added. To this tube, 12 mL of the hydrolyzed TPM was added in one shot. This mixture was then gently rotated overnight for 16 hours. To a 250 mL pyrex glass bottle, 40 mL of 100 mM NaOH, 40 mL of DI water, and 100 μL of Darocur were added and shaken for a minute. To this mixture, 20 mL of the aged TPM emulsion was added and immediately capped. The bottle was gently rotated for roughly 30 seconds before being placed in the UV reactor for 30 minutes. Again, the particles were washed in DI water by centrifuging 5 times.

Thermogravimetric analysis (TGA). TGA measurements were conducted on a Discovery TGA 550 (TA Instruments, USA). Dispersions of hollow particles (HP1 and HP2) were dried to obtain solid samples. Approximately 2 mg of dried material was loaded into a platinum pan and heated from 25 to 800 °C at a rate of 10 °C min^{-1} under an air atmosphere. The residual mass at 800 °C was taken as the inorganic (silica) content of the particles (see **Figure S1**), showing silica content of 26 and 29 wt.% for HP1 and HP2, respectively.

Dynamic and Electrophoretic Light Scattering (DLS-ELS). Particle size distribution and ζ-potential measurements for HP, TiO_2 and binder particles (**Figure S2** and **Table 1**) were performed using a Zetasizer Ultra (Malvern Panalytical, Malvern, U.K.). The measurements were carried out at 25 °C in folded capillary cells (DTS1070), and three repetitions were performed for each sample.

Table 1: Physical characteristics of the particles used in this study: diameter, ζ-potential, and shell thickness.

Particle	Diameter[a] (D_H, µm)	ζ[b] (mV)	Shell thickness[c] (nm)
HP1	5.0 ± 0.5	-66 ± 1	250
HP2	1.0 ± 0.2	-45 ± 1	200
TiO_2 P25	0.5 ± 0.2	25 ± 1	-
-Binder	0.0948 ± 0.0005	-54 ± 1	-
+Binder	0.0899 ± 0.0009	54 ± 2	-

[a]hydrodynamic diameter as measured by DLS; standard deviation derived from 3 average values; [b]zeta potential as measured by ELS; [c]as measured from SEM images of burst capsules (**Figure S3)**.

Coatings formulation and formation. The appropriate opacifier dispersion (HPs or TiO_2) amounts were mixed with either positively or negatively charged binder particles in Milli-Q water and the blend was vortexed for a few seconds. Formulations of the different particle blends in this study can be found in **Table 2**. All formulations were prepared to have the same wt.% of opacifier. Please note that in the case of HPs this includes the water contained within their core. 400 µL of the opacifier/binder blend were cast on square glass coverslips (18 mm × 18 mm), previously cleaned with an ultraviolet ozone cleaner (Ossila, Sheffield) for 10 minutes. Then they were left to film form in an environmental chamber (HPP IPP plus, Memmert, Germany) at 25 ± 1 °C and three different relative humidities: RH 90 ± 1% (slow evaporation), RH 50 ± 1% (intermediate evaporation), or RH 15 ± 1% (fast evaporation). The evaporation rates were determined via gravimetric experiments as 1.15×10^{-7} m s^{-1}, $7.85 \times 10^{-}$

^{8} m s^{-1}, and 9.29 × 10^{-9} m s^{-1} for fast, intermediate and slow evaporation, respectively (see **Figure S4** for details).

Table 2: Coatings formulations: weight percentages (wt.%) and volume fractions (φ) of opacifiers (HP1, HP2, or TiO_2) and polymeric binders in the dispersion.

Opacifier	**wt.% [a]**	**wt.% solids[b]**	**$\varphi_{opacifier}$[c]**	**Binder**	**wt.% solids[d]**	**φ_{binder}[e]**
HP1	1.2	0.3	0.012		1.8	0.016
HP2	1.2	0.9	0.012		1.8	0.016
TiO_2	1.2	1.2	0.003		1.8	0.016

[a]including water in HPs' cores; [b]excluding water in HP's cores; [c]opacifier volume fraction; [d]solids content of binder particles; [e]binder volume fraction.

Scanning Electron Microscopy (SEM) and Energy-Dispersive X-ray Spectroscopy (EDS). Cross-sectional images of the coatings were acquired using a JEOL JSM-7100F field emission gun scanning electron microscope. Films were fractured by exerting force while holding them with two pairs of flat tweezers and then sputter coated with gold and palladium to improve conductivity. Elemental analysis and EDS maps were acquired using an Oxford Instruments X-Max^{N} 80 mm^2 detector. An accelerating voltage of 5 keV and a probe current of approximately 200 pA were used for SEM imaging, while an accelerating voltage of 10 keV and a probe current of approximately 1 nA were used for EDS.

Transmittance and Reflectance measurements. Transmittance and reflectance (both total and diffuse) of the coatings in the 400–2500 nm spectral range were measured using a UV–

vis–NIR spectrophotometer (Cary 5000, Agilent Technologies, USA) equipped with an internal integrating sphere (Diffuse Reflectance Accessory DRA-2500). A tungsten–halogen lamp was used as the light source for the Vis–NIR region. Total reflectance consists of both diffuse and specular components. Specular reflectance is associated with mirror-like reflections, where light is reflected at a specific angle, whereas diffuse reflectance results from multiple scattering events within the coating, leading to reflection in all directions.[20] A polytetrafluoroethylene (PTFE) reflectance standard disk was used as the 100% reflectance reference. Measurements were performed at a wavelength scanning rate of 500 nm min^{-1}. For each sample, three independent measurements were performed by repositioning the sample on the integrating sphere opening each time to account for potential inhomogeneities. The reported values represent the mean reflectance or transmittance, and the error bars indicate the standard deviation across these three measurements.

Optical microscopy. A Keyence VHX-7000N digital microscope equipped with a VHX-E20 high-resolution low-magnification objective lens was used to visualize the surface of the coatings. To capture the entire 18 mm × 18 mm area, four individual images were acquired and subsequently stitched together using the VHX software provided with the microscope.

3. RESULTS AND DISCUSSION

3.1 Interactions between hollow and binder particles

Initially, the interaction of HPs with binder particles was investigated using DLS (**Figure 1**). A dispersion of HPs ($\varphi = 1\times10^{-3}$ or 1×10^{-4} for HP1 and HP2 respectively) was mixed with increasing volume fractions of binder particles, which were either negatively or positively charged. For HP1, we estimated that full surface coverage would be achieved for N_{ratio} (binder particles per HP particle) above 1×10^{4} (see **Table S1**). For HP2, full coverage would be reached for $N_{ratio} > 4\times10^{2}$. When both HP and binder particles were negatively charged, in DLS

measurements a peak located at around 100 nm remained, indicating the presence of free binder particles in the dispersion **(Figure 1 A** and **C**). When binder particles were positively charged, the peak corresponding to free binder particles was not present **(Figure 1 B** and **D**) even at concentrations below the theoretical full surface coverage. This suggests binder particle adsorption on the surface of HPs. At higher concentrations, binder particles are present in excess and thus their peak is visible. In blends of HP2 and positively charged binder, indications of large aggregate formation were observed as the binder particle concentration increased **(Figure 1D)**. A similar aggregation phenomenon is suspected for HP1, although the resulting structures may be larger than the detection window of the instrument, not allowing for their direct observation.

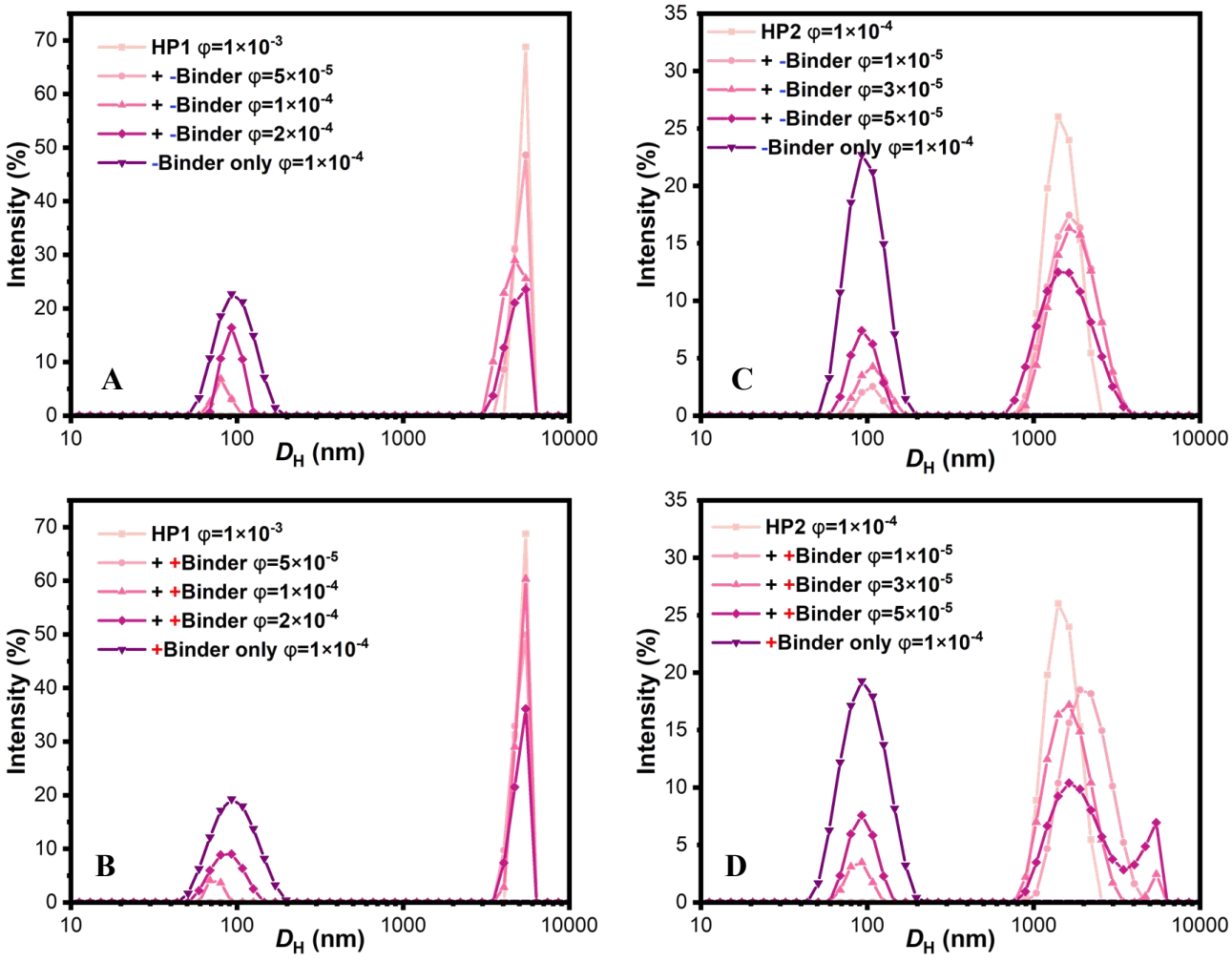

Figure 1: Intensity distributions vs hydrodynamic diameter of hollow particles (HPs) dispersion upon addition of negatively or positively charged polymeric binder particles.

3.2 Coating formation and factors influencing colloidal assembly

To investigate the influence of HP content on film structure and optical properties, three different HP:binder ratios were tested: 20:80, 30:70, and 40:60, expressed as wt.% in the dried coating. Optical microscopy images of coatings with different opacifiers (HP or TiO_2) and binder particles (negatively or positively charged) at the different opacifier:binder ratios are presented in **Figure S5**. At first sight, all of these are highly opaque whereas binder-only coatings are transparent (**Figure S6**). In all cases, the amount of binder particles is over the minimum to achieve full surface coverage of the HPs, to ensure film formation. Reflectance measurements (**Figure S7**) confirmed that, as expected, increases in HP content led to higher total reflectance. After verifying this trend, the highest HP content (HP:binder = 40:60) was chosen for further studies.

It is known that the distribution of particles across the thickness of a coating can impact its optical properties. For example, a gradually decreasing local volume fraction of particles from the top to the bottom of a coating has been shown in simulation studies to enhance reflectance.[35,36] The final distribution of particles in a colloidal film is determined by the interplay of various physical and/or physicochemical processes, namely solvent evaporation, particle diffusion and adsorption at interfaces, sedimentation, and diffusiophoresis (if chemical gradients are present). The Péclet number (*Pe*) serves as a first indicator for the balance between evaporation and diffusion in a system:[37]

$$P_e = \frac{H_0 \dot{E}}{D_0} \qquad Eq.1$$

where H_0 is the wet film height, $\dot{E}$ the evaporation rate, and D the Stokes-Einstein diffusion coefficient obtained via:

$$D_0 = \frac{kT}{6\pi\mu R} \qquad Eq.2$$

where R is the particle radius, μ the solvent's viscosity, k the Boltzmann's constant, and T the temperature in Kelvin. When Pe < 1, diffusion dominates, allowing particles to move freely while the coating is drying. When Pe > 1, evaporation dominates, leading to particle accumulation at the air-water interface.[38] In our system, because of the large diameter of the HPs, we expect to observe sedimentation effects. These can be accounted for using the sedimentation Péclet number (Pe_{sed}):

$$P_{e_{sed}} = \frac{H_0 U_0}{D_0} \qquad Eq.3$$

where U_0 is the Stokes settling velocity given by:

$$U_0 = \frac{2R^2 g(\rho_p - \rho_L)}{9\mu} \qquad Eq.4$$

where g is the gravitational acceleration, and ρ_p and ρ_L the densities of the particle and dispersing medium, respectively. A sedimentation number (N_s) can be used to evaluate the balance between sedimentation and evaporation:

$$N_s = \frac{U_0}{\dot{E}} \qquad Eq.5$$

When $N_s >> 1$, sedimentation is expected to dominate and if $N_s < 1$, evaporation is expected to dominate, while $N_s \sim 1$ points to an intermediate scenario.

Pe, Pe_{sed} and N_s have been calculated for HP1 and HP2 in our formulations and can be seen in **Table 3**. The same calculations have been performed for the binder particles (see results in **Table S2**). We will now present our findings on the microstructure of the films and correlate them with these parameters to unveil the processes underlying their assembly.

Table 3: Evaporation rate ($\dot{E}$), Péclet number (Pe), sedimentation Péclet number (Pe_{sed}) and sedimentation number (N_s) obtained from equations S1, 1, 3 and 5, respectively, for HP1 and HP2 at 25 °C and the different relative humidity conditions used in this study. In the presence of positively charged binder particles, the size of HP was approximated as $R_{HP} + 2R_{binder}$, in line with the DLS evidence for the formation of raspberry-like structures.

Sample name	**Size (µm)**	**Binder surface charge**	**RH (%)**	$\dot{E}$ **(× 10^{-7} m/s)**	**Pe**	**Pe$_{Sed}$**	**N$_s$**
	HP1						
HP1_Neg_RH15	5.0 ± 0.5	-	15	1.15	1530 ± 150	2610 ± 760	1.6 ± 0.3
HP1_Neg_RH50			50	0.78	1000 ± 100	2610 ± 760	2.5 ± 0.5
HP1_Neg_RH90			90	0.09	119 ± 12	2610 ± 760	22 ± 4
HP1_Pos_RH15	5.2 ± 0.5	+	15	1.15	1590 ± 150	2930 ± 830	1.8 ± 0.3
HP1_Pos_RH50			50	0.78	1040 ± 100	2930 ± 830	2.8 ± 0.5
HP1_Pos_RH90			90	0.09	123 ± 12	2930 ± 830	23.4 ± 4.5
	HP2						
HP2_Neg_RH15	1 ± 0.2	-	15	1.15	293 ± 58	75 ± 40	0.24 ± 0.09
HP2_Neg_RH50			50	0.78	200 ± 40	75 ± 40	0.34 ± 0.13
HP2_Neg_RH90			90	0.09	24 ± 5	75 ± 40	2.9 ± 1.1

HP2_Pos_RH15	1.2 ± 0.2	+	15	1.15	352 ± 59	126 ± 59	0.34 ± 0.11
HP2_Pos_RH50			50	0.78	240 ± 40	126 ± 59	0.50 ± 0.16
HP2_Pos_RH90			90	0.09	29 ± 5	126 ± 59	4.2 ± 1.4

3.3 Coatings microstructure

SEM cross-sectional imaging was carried out to determine particle distributions within the coatings and establish correlations with the theoretical calculations presented in **Table 3**. In all the systems, N_s for binder particles is always smaller than 1 (see **Table S2**). This means they do not experience sedimentation and thus they are more likely to be trapped at the air/water interface when evaporation dominates. For both HP1 and HP2, in samples dried at 90% relative humidity the calculated sedimentation number was $N_s >> 1$, indicating that sedimentation of HPs during film formation was expected. The visualization via SEM of small-on-top structures in the coatings formed under these conditions confirmed this scenario, where HPs accumulate near the substrate and binder particles form the upper layer (**Figures 2C, 2F, 3C, and 3F**). At 50% RH, N_s values for HP1 fluctuate around 2, making it uncertain whether a segregated or mixed particle scenario is expected. Experimentally, a homogeneous particle distribution was observed when blending negatively charged binder particles with HP1 (**Figure 2B**), whereas for the positively charged binder blend there was a clear segregation into a small-on-top structure (**Figure 2E**). These findings suggest that we might have reached a critical transition point for the system at 50% RH, with the adsorption of binder particles on the HPs resulting in an increase in HP particle size and mass which tips the balance towards a sedimentation-driven assembly.

For the remaining systems we now enter the region where, rather than competing between evaporation and sedimentation, the two main players are evaporation and diffusion. All coatings formed at 15% RH present a clear small-on-top structure when imaged by SEM (**Figures 2A, 2D, 3A and 3D**). This observation, together with the high P_e/low N_s numbers for these systems, points towards a vertical size segregation induced by the trapping of binder particles at the air/water interface and the subsequent diffusiophoresis of HPs towards the substrate.[39–41] In HP2-containing formulations at 50% RH, we observe how by changing the surface charge of the binder we can switch from a homogeneous HP distribution (positively charged latex, **Figure 3E**) to a small-on-top structure (negatively charged latex, **Figure 3B**), likely due to the formation of raspberry-like structures in the first case.

All HP2-based coatings showed a slight edge-thickening (coffee-ring effect) pattern where the outer ~2 mm of each 18×18 mm coating was thicker, with uniform thickness beyond that. The only exception was the HP2_Pos_RH90 sample, which showed a more pronounced edge – center thickness difference and thickness inhomogeneities (see **Figure S8**). In contrast, HP1 coatings dried with uniform thickness and no detectable ring. The SEM images of the cross-section reveal thickness differences towards the edge region. In this case, binder particle-rich zones appeared near the edges, where a visibly thicker binder layer extends from left to right. Anyfantakis et al.[42] reported that coffee-ring effect occurred in blends of surfactants and particles when they were oppositely charged, and the surfactant concentration was high (similar to our HP2 with positive binder in excess case). This led to surfactant adsorption on the particle surface and charge reversal of the particles. In the HP2_Pos_RH90 system, a similar phenomenon might be occurring, where under slow evaporation conditions, oppositely charged particles have more time to form raspberry-like aggregates. Raspberry-like particle formation is often time-dependent, where longer interaction times favour heteroaggregate formation,[43] which is in alignment with our observation.

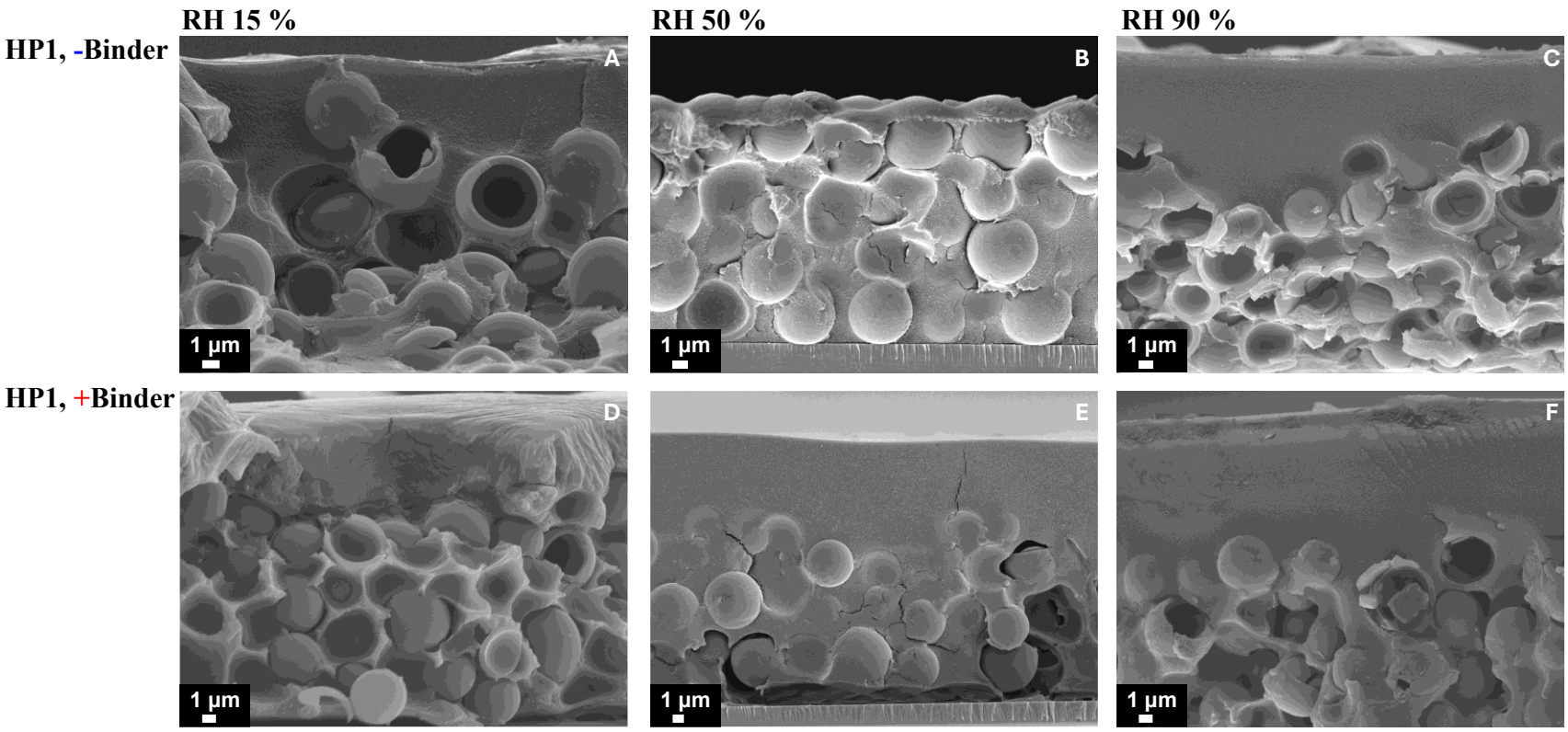

Figure 2. SEM images of cross-sectioned fractured coatings containing HP1 and negatively or positively charged binder polymer particles dried at 15, 50 or 90% relative humidity (RH%).

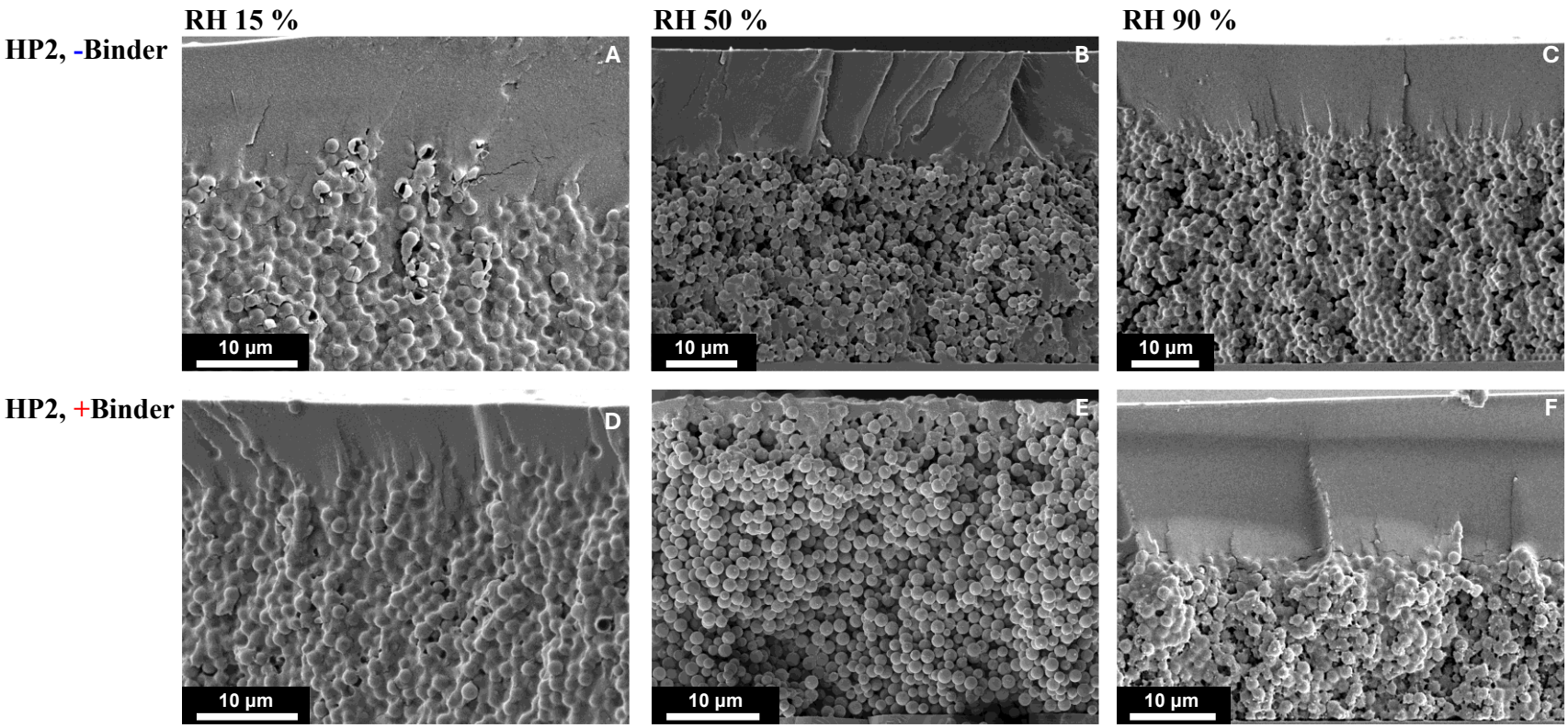

Figure 3: SEM images of cross-sectioned fractured coatings containing HP2 and negatively or positively charged binder polymer particles dried at 15, 50 or 90% relative humidity (RH%).

3.3 Optical properties

Opacity refers to the ability of a coating to hide or obscure the surface underneath it. It is a measurement of how effectively the coating prevents light from passing through to the substrate. Therefore, both transmission and reflectance measurements provide quantitative assessments of a coating's hiding power. HP-containing coatings were compared against reference TiO_2-containing coatings dried under the same environmental conditions. Cross-sectional SEM images of these reference films can be found in **Figure S9**. The microstructure of the reference films varies depending on the environmental conditions, resulting in either a small (binder)-on-top configuration or a homogeneous distribution of TiO_2. These finding were confirmed via EDS elemental analysis (**Figure S10**).

Transmission spectra across the visible to near-infrared region (400–2500 nm) for the HP-containing and the reference TiO_2-containing coatings are presented in **Figure 4**. Three initial observations can be made from the data. First, the HP coatings block light over a broader spectral range when compared to TiO_2-containing coatings, particularly in the NIR region. Second, HP2-containing coatings exhibit significantly lower transmittance compared to those containing HP1. Third, the variation in transmittance among samples formulated with the same opacifier is relatively small, with the exception of HP2_Pos_RH90.

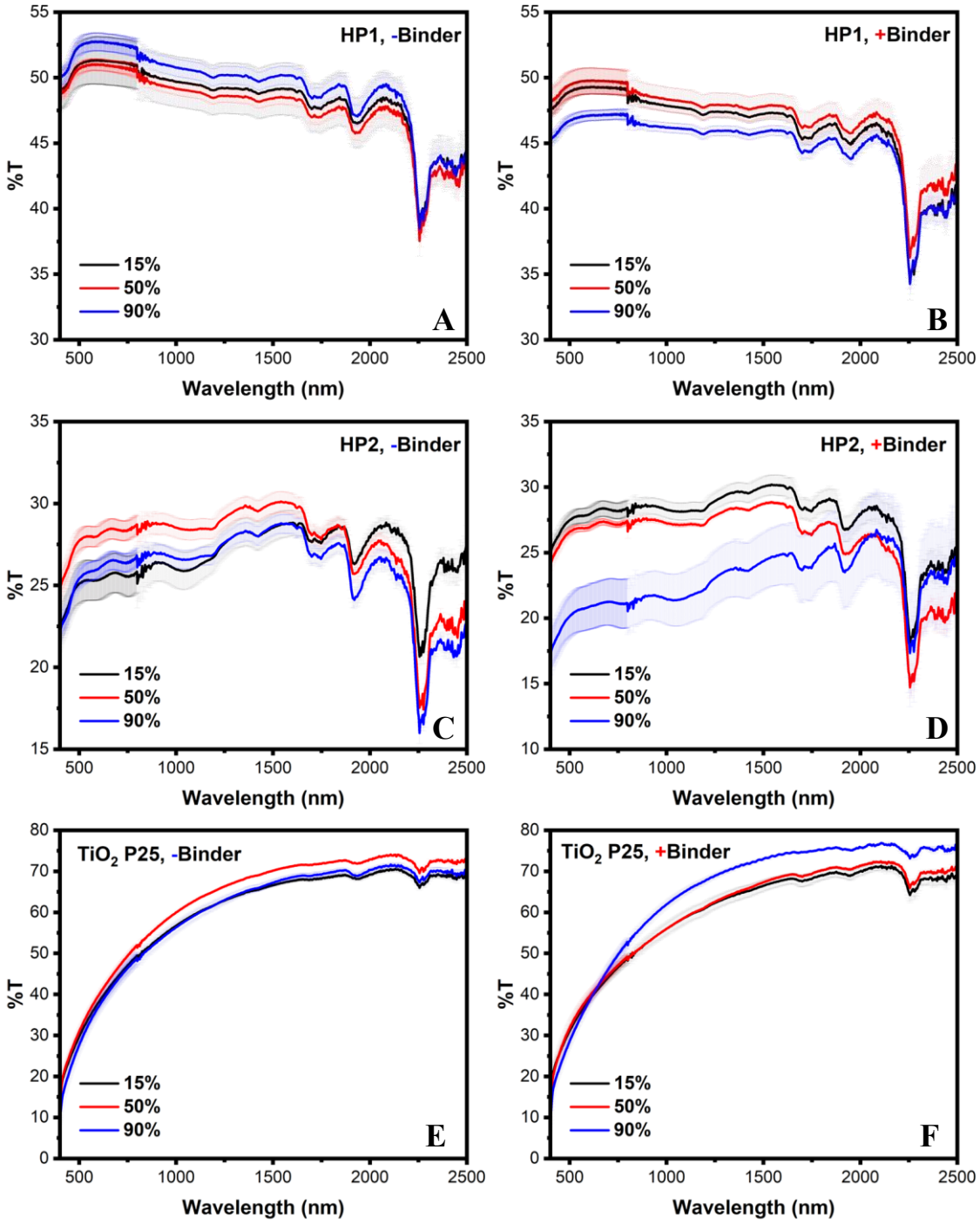

Figure 4: Vis-NIR transmission spectra of the HP-containing coatings and the TiO_2-containing reference coatings dried at 25 ºC and different relative humidities (15, 50 or 90%).

The total reflectance spectra of the HP coatings and the TiO_2 reference coatings are presented in **Figure 5**, while the diffuse reflectance spectra are presented in **Figure S11**. By comparing **Figure 5** and **Figure S11**, it is evident that almost all reflectance from our coatings is diffuse. This is expected due to the multiple scattering events occurring within the HPs. Reflectance spectra of binder-only films are shown in **Figure S6**.

Overall, HP2-containing films exhibited significantly higher reflectance than HP1-containing films. Literature suggests that decreasing the shell thickness enhances scattering efficiency, as it increases the interface-to-volume ratio.[44] Also, multiple scattering typically decreases as the particle diameter increases, but there is an optimal size for maximum efficiency.[21] HP2 has a smaller overall size and a thinner shell, which may explain its superior reflectance performance. Something worth noting is that, as shown in **Figure 5**, HPs exhibited much broader spectral reflectance than TiO_2, particularly in the NIR region, which can be an advantageous feature for applications requiring better thermal insulation.

For films from blends of HP2 with negatively charged binder, no significant difference in reflectance was observed within the experimental error. In HP1-containing films with negatively charged binder, reflectance variations appear to be associated with differences in HP distribution across the film thickness (**Figure 2**). Measured thicknesses for each coating (without taking into account the coffee-ring region in the HP2 coatings), determined from SEM images, are summarized in **Table 4**. The measured thicknesses of the three coatings were: for 15% RH, 19.1 ± 0.5 μm, for 50% RH, 16.4 ± 0.7 μm and for 90% RH, 23.5 ± 0.9 μm. In principle, an increase in coating thickness should lead to higher reflectance.[45] However, HP1_Neg_50 exhibited the highest reflectance despite having the smallest thickness. This suggests that the homogeneous HP distribution observed in this coating, and thus a homogenous distribution of scattering centres,

results in the higher reflectance measured. Is has been reported that when optically scattering particles are agglomerated or closely packed, the overall reflectance of the coating can decrease as a result of a reduced scattering efficiency.[46]

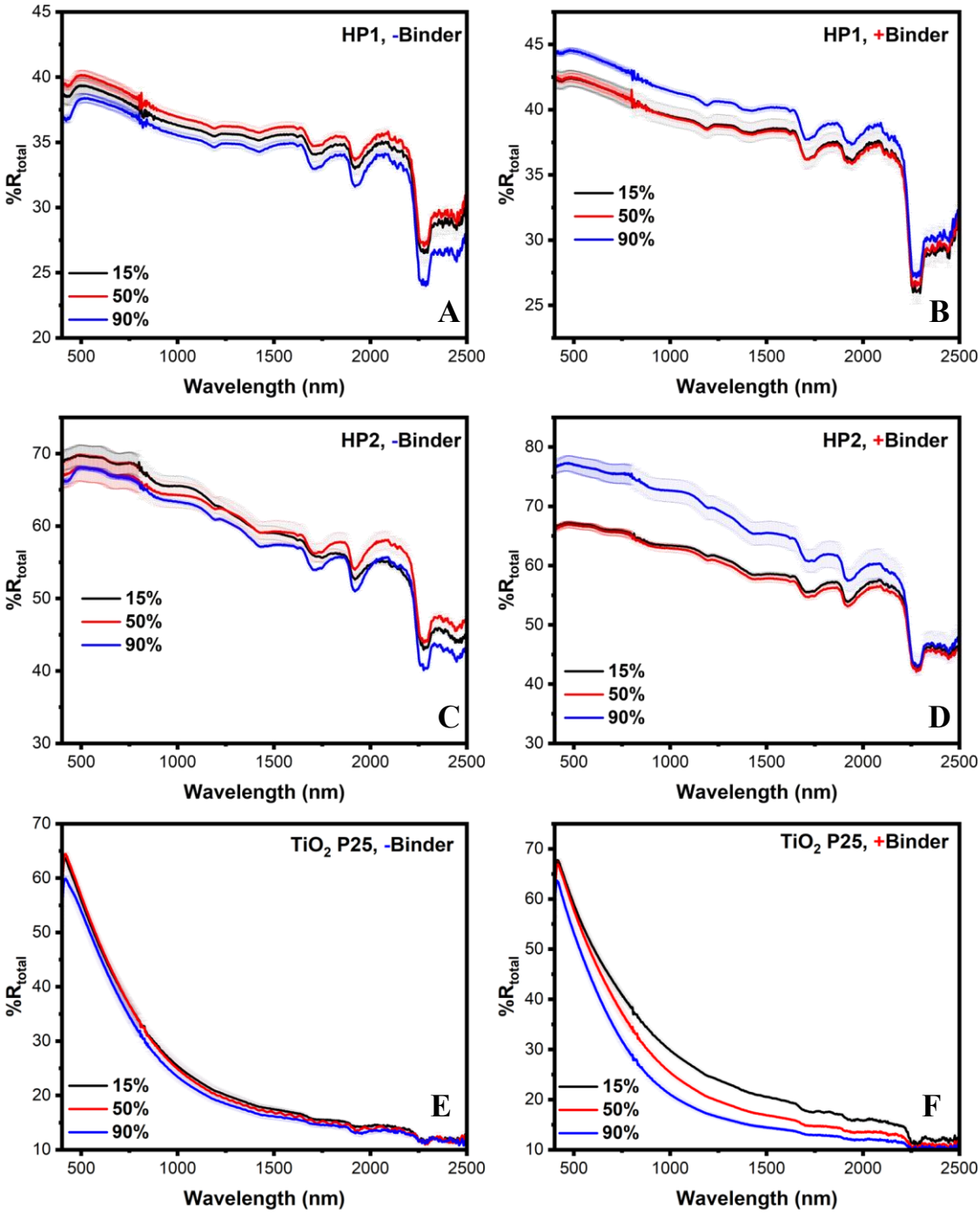

Figure 5: Vis-NIR total reflectance spectra of HP-containing and TiO_2 reference coatings formed at 25 ^oC and different relative humidities (15, 50 or 90%).

Coatings formed at 15 and 50% RH containing either positive or negatively charged binder showed comparable reflectance. However, at 90% RH coatings with positively charged binder showed significantly higher reflectance. Since no significant difference in thickness was observed (**Table 4**), this enhanced scattering is likely due to differences in film microstructures rather than coating thicknesses. The longer drying time at high RH is likely to enable the formation of more raspberry-like HP-binder structures, increasing separation between HP particles and enhancing light scattering efficiency.

The differences in reflectance among TiO_2-containing coatings were likely influenced by both variations in thickness (**Table 4**) and particle distribution (**Figure S9** and **Figure S10**). Despite the thickness differences when film-formed with the negative binder, the overall reflectance remained relatively constant. This suggests variations in thickness might compensate for differences in TiO_2 particle distribution. For example, for the coating with negative binder dried at 15% RH, the increased thickness appeared to counterbalance the accumulation of TiO_2 particles at the bottom of the coating. In the case of TiO_2 and positively charged binder, TiO_2 was homogeneously distributed throughout the coating thickness (**Figure S9** and **Figure S10**), and therefore variations in reflectance are primarily attributed to thickness differences (**Table 4**).

Table 4: Coatings thickness as calculated from SEM images. For coatings with HP2 presenting coffee-ring effect, the thickness is taken from the area of the coating without the coffee-ring.

Binder surface charge	RH (%)	With HP1 (µm)	With HP2 (µm)	With TiO_2 (µm)
-	15	19.1 ± 0.5	24 ± 2	35 ± 2
	50	16.4 ± 0.7	35 ± 2	28 ± 1
	90	23.5 ± 0.9	32 ± 4	15 ± 1
+	15	20 ± 1	32 ± 2	24 ± 3
	50	22 ± 3	30 ± 3	20 ± 1
	90	20 ± 2	30 ± 5	17 ± 1

To investigate further the potential application of HP-containing films as solar reflective coatings, we calculated their solar reflectance (R_{sun}). This figure of merit represents the fraction of solar radiation which is reflected by a surface. The average solar reflectance of the coatings was calculated using a custom Python script that convolves the reflectance spectra with the standard solar spectrum over the 400–2500 nm wavelength range as follows:[47,48]

$$R_{sun} = \frac{\int_{400}^{2500} R(\lambda) I_{sun}(\lambda) d\lambda}{\int_{400}^{2500} I_{sun}(\lambda) d\lambda} \qquad Eq. 6$$

where $R(\lambda)$ is the reflectance spectrum of the coating and $I_{sun}(\lambda)$ the solar spectral radiation as per ASTM G173-03 standard[49]. The Jupyter Notebook containing the Python code used for this calculation is provided as a Supporting Information file. The calculated average solar reflectance

values for the coatings are presented in **Table 5**. HP1-containing coatings exhibited values comparable to the reference TiO_2-containing coatings, with reflectance in the range of 30–40%. HP2-containing coatings showed significantly higher solar reflectance, ranging from 64–73%.

Overall, solar reflectance values where mostly dependent on the opacifier used (HP1, HP2, or TiO_2) rather than its distribution within the coating. This suggests that the overall coating composition and the presence of a sufficient concentration of HPs throughout the film still enable effective optical performance across a range of film forming conditions and binders. A plausible explanation is that the high scattering efficiency of HPs dominates the overall optical coating response, and that the size, refractive index contrast, and multiple scattering paths enabled by the hollow geometry may mitigate the impact of microstructural differences.

Such robustness in optical performance could be advantageous from an industrial perspective. It implies that high reflectance, and by extension, opacity and solar reflectance, can be achieved without extremely tight control over drying conditions or particle distribution. This characteristic enhances their industrial appeal, as it allows for less restricted drying conditions without compromising efficiency.

Table 5: Solar reflectance (R_{sun}) of the coatings calculated via Eq. 6.

Opacifier	**Binder**	**RH (%)**	**R_{sun} (%)**
HP1	-	15	37.5
		50	38.2

		90	36.6
	+	15	40.6
		50	40.5
		90	42.5
HP2	-	15	66.4
		50	65.2
		90	64.5
	+	15	64.3
		50	63.9
		90	73.3
TiO_2 (P25)	-	15	37.8
		50	37.8
		90	35.8
	+	15	41.4
		50	38.5
		90	34.2

CONCLUSIONS

In this work, we explored the use of hybrid polymer-silica HPs as replacement for TiO_2 opacifiers in coatings formulations. We investigated two types of HPs that differed in size and shell thickness. Each type was combined with either like charged or oppositely charged polymeric binder particles to form coatings. These coatings were dried under different relative humidity conditions, resulting in distinct microstructures and optical properties.

The interactions of HPs with binder particles in the formulations were examined with DLS, showing complexation in systems with oppositely charged particles, and excess of free binder particles when their concentration was above full surface coverage. Reflectance measurements across the Vis–NIR spectrum demonstrated that increasing HP concentration enhanced light-scattering performance. Transmittance and reflectance measurements showed that the smaller HPs (HP2) consistently outperformed both the larger HPs (HP1) and the reference TiO_2. Notably, they achieved average solar reflectance values of up to 73.3%. This result highlights the potential of these HPs not only as opacifiers but also for use in solar reflective coatings. The enhancement is attributed to HP2 optimized architecture - their smaller size and thinner shell - which facilitates multiple internal scattering events.

SEM imaging of the coatings cross-sections revealed that particle distribution varied with relative humidity, surface charge, and opacifier type (HP1, HP2, or TiO_2). We found out that the balance between diffusion, evaporation, and sedimentation processes determines the final film morphology. These structural differences of the coatings were correlated with variations in optical performance, highlighting the critical role of formulation and processing conditions on the final optical behavior of the coatings.

Through control of particle size, shell thickness, and formulation parameters, we achieved coatings with reflectance comparable to or exceeding that of TiO_2-containing systems. In addition to excellent opacifying properties, hybrid polymer-silica HPs demonstrated broader spectral transmittance and reflectance compared to TiO_2, particularly in the NIR region – a valuable property for thermal insulation and surface cooling applications.

To the best of our knowledge, this study is the first to demonstrate the full replacement of TiO_2 in opacifying coatings using polymer-based HPs for a comparable performance in the vis-NIR range. Lastly, the minimal variation in reflectance despite differences in microstructure suggests that the performance of HPs is not significantly influenced by particle distribution within the coatings, a characteristic with high industrial appeal, as it allows greater flexibility in drying conditions without compromising efficiency. Our findings highlight the potential of hybrid polymer-silica HPs as a more sustainable, high-performance alternative to conventional metal oxide opacifiers and pave the way for their broader implementation in energy-efficient and environmentally friendly coating technologies. Future work will focus on conducting life cycle assessment studies to evaluate the environmental impact of HPs in comparison with TiO_2, as well as their stability under high shear conditions present in industrial formulation processes. Moreover, testing the mechanical properties (e.g., abrasion resistance, adhesion, long-term stability under weathering) of the HP-containing films will be key to accelerate the industrial adoption of these HPs.

ASSOCIATED CONTENT

Supplementary data

Synthesis of binder particles; thermogravimetric analysis; intensity vs hydrodynamic diameter of particle dispersions; SEM images of burst HPs; evaporation rate calculations; surface coverage calculations; optical microscopy images of opacifier-containing coatings; optical microscopy images and reflectance of binder only coatings; total reflectance spectra of coatings with different HP:binder ratios; binder Péclet numbers, sedimentation Péclet numbers, and sedimentation numbers; SEM images of coatings presenting coffee-ring effect; SEM images of TiO_2 coatings; SEM images and EDS maps of TiO_2 coatings; diffuse reflectance spectra of coatings.

Jupyter notebook demonstrating reflectance calculations.

AUTHOR INFORMATION

Corresponding Author

Constantina Sofroniou - Department of Materials, Loughborough University, Loughborough LE11 3TU, United Kingdom; orcid.org/0000-0002-4990-0371; Email: c.sofroniou@lboro.ac.uk

Authors

Sarah Chong - Department of Chemistry, New York University, NY 10003-6688 New York, USA; orcid.org/0000-0002-2859-626X; Email: swc8706@nyu.edu

Timothy James Murdoch - Department of Materials, Loughborough University, Loughborough LE11 3TU, United Kingdom; orcid.org/0000-0001-8727-0908; Email: t.j.murdoch@lboro.ac.uk

Edgar Espinosa Rodriguez - Universite Claude Bernard Lyon 1, CPE Lyon, CNRS, UMR 5128, Catalysis, Polymerization, Processes and Materials (CP2M), 69616 Villeurbanne Cedex, France; Email: edgar.espinosa-rodriguez@univ-lyon1.fr

Franck D'Agosto - Universite Claude Bernard Lyon 1, CPE Lyon, CNRS, UMR 5128, Catalysis, Polymerization, Processes and Materials (CP2M), 69616 Villeurbanne Cedex, France; orcid.org/0000-0003-2730-869X; Email: franck.dagosto@univ-lyon1.fr

Muriel Lansalot - Universite Claude Bernard Lyon 1, CPE Lyon, CNRS, UMR 5128, Catalysis, Polymerization, Processes and Materials (CP2M), 69616 Villeurbanne Cedex, France; orcid.org/0000-0001-9010-6746; Email: muriel.lansalot@univ-lyon1.fr

Stefano Sacanna - Department of Chemistry, New York University, NY 10003-6688 New York, USA; orcid.org/0000-0002-8399-3524; Email: s.sacanna@nyu.edu

Ignacio Martín-Fabiani - Department of Materials, Loughborough University, Loughborough LE11 3TU, United Kingdom; orcid.org/0000-0002-1977-7659; i.martin-fabiani@lboro.ac.uk

Author Contributions

CS: Conceptualization, Methodology, Data collection, Curation and Analysis, Validation, Visualization, Writing (Original draft, Review and Editing). **SC**: Resources (hollow particles), Writing (Original draft - HP synthesis, Review and Editing). **TJM**: Data Analysis (Python code), Writing (Review and Editing). **EER**: Resources (binder particles), Writing (Original draft - binder synthesis, Review and Editing). **FD**: Resources (binder particles), Writing (Original draft - binder synthesis, Review and Editing). **ML**: Resources (binder particles), Writing (Original draft - binder synthesis, Review and Editing). **SS**: Resources (hollow particles), Writing (Review and Editing).

IMF: Conceptualization, Supervision, Resources, and Writing (Review and Editing). All authors have read and approved the final manuscript.

Declaration of competing interest

The authors declare no competing financial interest.

ACKNOWLEDGMENT

The authors are grateful for support from UK Research and Innovation in the form of a Future Leaders Fellowship (MP/ T02061X/1), which is supporting both I. M.-F. and C.S. The authors would also like to thank the Loughborough Materials Characterization Centre's team and Dr. Keith Yendall for technical assistance with SEM characterization. S.S. and S.W.C. were supported by the U.S. Department of Energy, Office of Science, Office of Basic Energy Sciences under Award Number DE-SC0020971.

REFERENCES

[1] A.S. Fonseca, A.K. Viitanen, T. Kanerva, A. Säämänen, O. Aguerre-Chariol, S. Fable, A. Dermigny, N. Karoski, I. Fraboulet, I.K. Koponen, C. Delpivo, A.V. Villalba, S. Vázquez-Campos, A.C. Østerskov Jensen, S.H. Nielsen, N. Sahlgren, P.A. Clausen, B.X. Nguyen Larsen, V. Kofoed-Sørensen, K.A. Jensen, J. Koivisto, Occupational exposure and environmental release: The case study of pouring tio2 and filler materials for paint production, Int. J. Environ. Res. Public Health 18 (2021) 1–26. https://doi.org/10.3390/ijerph18020418.

[2] M.P. Diebold, Optimizing the benefits of TiO2 in paints, J. Coatings Technol. Res. 17 (2020) 1–17. https://doi.org/10.1007/s11998-019-00295-2.

[3] N.S. Bischoff, M.R. Bussi, S.G. Van Breda, S. Jolani, D.T.H.M. Sijm, T.M. de Kok, J.J. Briedé, Food-grade titanium dioxide exposure between age groups and in global regions: a systematic review and meta-analysis, Crit. Rev. Food Sci. Nutr. 0 (2025) 1–11. https://doi.org/10.1080/10408398.2025.2467823.

[4] L. Palugan, M. Spoldi, F. Rizzuto, N. Guerra, M. Uboldi, M. Cerea, S. Moutaharrik, A. Melocchi, A. Gazzaniga, L. Zema, What's next in the use of opacifiers for cosmetic coatings of solid dosage forms? Insights on current titanium dioxide alternatives, Int. J. Pharm. 616 (2022) 121550. https://doi.org/10.1016/j.ijpharm.2022.121550.

[5] V. Pokharkar, S. Chandak, R. Pawar, A. Khandke, The implications of the EU ban on titanium dioxide: A comprehensive review of safety concerns and alternatives, Ann. Pharm. Françaises (2024). https://doi.org/10.1016/j.pharma.2024.11.002.

[6] R. Blundell, P. Butterworth, A. Charlier, D. Daurio, M. Degenhardt, D. Harris, B. Hancock, M. Johnston, R. Kasina, J. Kaye, R. Kelly, P. Lienbacher, L. Meehan, J. Melnick, P. Ojakovo, J. Schoell, B. Schimmelle, M. Tobyn, L. Wagner-Hattler, J. Wakeman, R. Wiedey, The Role of Titanium Dioxide (E171) and the Requirements for Replacement Materials in Oral Solid Dosage Forms: An IQ Consortium Working Group Review, J. Pharm. Sci. 111 (2022) 2943–2954. https://doi.org/10.1016/j.xphs.2022.08.011.

[7] M. Schutte-Smith, E. Erasmus, R. Mogale, N. Marogoa, A. Jayiya, H.G. Visser, Using visible light to activate antiviral and antimicrobial properties of TiO2 nanoparticles in paints and coatings: focus on new developments for frequent-touch surfaces in hospitals, J. Coatings Technol. Res. 20 (2023) 789–817. https://doi.org/10.1007/s11998-022-00733-8.

[8] H.M.F. Shakir, A. Ali, U. Zubair, T. Zhao, Z.A. Rehan, I. Shahid, Fabrication of low emissivity paint for thermal/NIR radiation insulation for domestic applications, Energy Reports 8 (2022) 7814–7824. https://doi.org/10.1016/j.egyr.2022.05.287.

[9] S. Sun, H. Ding, W. Ao, B. Zhang, Y. Liu, J. Zhang, H. Zhang, M. Li, A zirconium-free glaze system for sanitary ceramics with SiO2-CaCO3-TiO2 composite opacifier containing anatase: Effect of interface combination among SiO2, CaCO3 and TiO2, J. Eur. Ceram. Soc. 42 (2022) 2523–2534. https://doi.org/10.1016/j.jeurceramsoc.2021.12.069.

[10] Y. Zhao, C. Li, X. Liu, F. Gu, H. Jiang, W. Shao, L. Zhang, Y. He, Synthesis and optical properties of TiO2 nanoparticles, Mater. Lett. 61 (2007) 79–83. https://doi.org/10.1016/j.matlet.2006.04.010.

[11] Y. Dai, H. Dong, L. Sun, J. Li, T. Zhang, Y. Geng, Z. Liu, Life cycle environmental impact assessment of titanium dioxide production in China, Environ. Impact Assess. Rev. 105 (2024) 107412. https://doi.org/10.1016/j.eiar.2023.107412.

[12] M.J. Gázquez, S.M.P. Moreno, J.P. Bolívar, TiO2 as white pigment and valorization of the waste coming from its production, in: Titan. Dioxide Its Appl., Elsevier, 2021: pp. 311–335. https://doi.org/10.1016/B978-0-12-819960-2.00011-0.

[13] S. Middlemas, Z.Z. Fang, P. Fan, Life cycle assessment comparison of emerging and traditional Titanium dioxide manufacturing processes, J. Clean. Prod. 89 (2015) 137–147. https://doi.org/10.1016/j.jclepro.2014.11.019.

[14] A.A. Keller, H. Wang, D. Zhou, H.S. Lenihan, G. Cherr, B.J. Cardinale, R. Miller, J.I. Zhaoxia, Stability and aggregation of metal oxide nanoparticles in natural aqueous matrices,

Environ. Sci. Technol. 44 (2010) 1962–1967. https://doi.org/10.1021/es902987d.

[15] C.P. Tso, C.M. Zhung, Y.H. Shih, Y.M. Tseng, S.C. Wu, R.A. Doong, Stability of metal oxide nanoparticles in aqueous solutions, Water Sci. Technol. 61 (2010) 127–133. https://doi.org/10.2166/wst.2010.787.

[16] B. Hancock, D. Harris, J. Kaye, L. Meehan, J. Melnick, M. Tobyn, B. Gibbard, J. Grou, C.T. Guarino, M. Halota, M. Howard, C.L. Marshall, S. Varghese, H. Khaled, P. Butterworth, Titanium Dioxide (E171 Grade) and the Search For Replacement Opacifiers and Colorants: Supplier Readiness Survey, Case Studies and Regulatory Perspective, J. Pharm. Sci. 113 (2024) 1285–1298. https://doi.org/10.1016/j.xphs.2023.12.006.

[17] B.T.T. Pham, D. Nguyen, V.T. Huynh, E.H. Pan, B. Shirodkar-Robinson, M. Carey, A.K. Serelis, G.G. Warr, T. Davey, C.H. Such, B.S. Hawkett, Aqueous Polymeric Hollow Particles as an Opacifier by Emulsion Polymerization Using Macro-RAFT Amphiphiles, Langmuir 34 (2018) 4255–4263. https://doi.org/10.1021/acs.langmuir.7b03410.

[18] J.F.A. Silva, T.M.T. Carvalho, M.L. Almeida, P. Pereira, H. Sousa, J. Martins, L. Carvalho, F.D. Magalhães, Use of multi-hollow polyester particles as opacifying agent for injection-molded polyethylene, Polymers (Basel). 12 (2020) 1–9. https://doi.org/10.3390/POLYM12061331.

[19] R.A. Bhavsar, V.B. Raghavendra, Estimation of Organic Opacifier in Water-Based Architectural Coatings Using Dynamic Mechanical Thermal Analysis, J. Anal. Chem. 78 (2023) 1087–1096. https://doi.org/10.1134/S106193482308004X.

[20] K. Thananukul, C. Kaewsaneha, P. Sreearunothai, A. Petchsuk, S. Buchatip, W. Supmak,

B. Nim, M. Okubo, P. Opaprakasit, Biocompatible Degradable Hollow Nanoparticles from Curable Copolymers of Polylactic Acid for UV-Shielding Cosmetics, ACS Appl. Nano Mater. 5 (2022) 4473–4483. https://doi.org/10.1021/acsanm.2c00606.

[21] S. Atiganyanun, Use of hollow silica and titanium dioxide microparticles in solar reflective paints for daytime radiative cooling applications in a tropical region, J. Photonics Energy 11 (2021) 1–14. https://doi.org/10.1117/1.jpe.11.022103.

[22] H. Liu, H. Ma, J. Joo, Y. Yin, Contribution of multiple reflections to light utilization efficiency of submicron hollow TiO2 photocatalyst, Sci. China Mater. 59 (2016) 1017–1026. https://doi.org/10.1007/s40843-016-5127-7.

[23] A. Kowalski, M. Vogel, R.M. Blankenship, Sequential heteropolymer dispersion and a particulate materal obtainable therefrom, useful in coating compositions as a thickening and/or opacifying agent, US Patent, 4, 468, 498, 1984.

[24] M.J.A. Ruszala, N.A. Rowson, L.M. Grover, R.A. Choudhery, Low Carbon Footprint TiO2 Substitutes in Paint: A Review, Int. J. Chem. Eng. Appl. 6 (2015) 331–340. https://doi.org/10.7763/ijcea.2015.v6.505.

[25] S. Dong, J.Y. Quek, A.M. Van Herk, S. Jana, Polymer-Encapsulated TiO2for the Improvement of NIR Reflectance and Total Solar Reflectance of Cool Coatings, Ind. Eng. Chem. Res. 59 (2020) 17901–17910. https://doi.org/10.1021/acs.iecr.0c03412.

[26] K. Dornelles, R. Caram, E. Sichieri, Natural weathering of cool coatings and its effect on solar reflectance of roof surfaces, Energy Procedia 78 (2015) 1587–1592. https://doi.org/10.1016/j.egypro.2015.11.216.

[27] E. Poshtkouhian Bavi, S. Nouri Jouybari, F. Mousavi, A rapid method for producing highly diffuse reflective white paint as the back surface reflector in dye-sensitized solar cell, Opt. Mater. (Amst). 131 (2022) 112647. https://doi.org/10.1016/j.optmat.2022.112647.

[28] C.M. Cardinal, L.F. Francis, L.E. Scriven, Drying and collapse of hollow latex, J. Coatings Technol. Res. 6 (2009) 457–469. https://doi.org/10.1007/s11998-009-9167-3.

[29] S. Nuasaen, P. Tangboriboonrat, Optical properties of hollow latex particles as white pigment in paint film, Prog. Org. Coatings 79 (2015) 83–89. https://doi.org/10.1016/j.porgcoat.2014.11.012.

[30] R.A. Ramli, Hollow polymer particles: A review, RSC Adv. 7 (2017) 52632–52650. https://doi.org/10.1039/c7ra10358a.

[31] Z. Xu, T. Hueckel, W.T.M. Irvine, S. Sacanna, Transmembrane transport in inorganic colloidal cell-mimics, Nature 597 (2021) 220–224. https://doi.org/10.1038/s41586-021-03774-y.

[32] X. Chen, S.S. Mao, Titanium Dioxide Nanomaterials: Synthesis, Properties, Modifications, and Applications, Chem. Rev. 107 (2007) 2891–2959. https://doi.org/10.1021/cr0500535.

[33] M.A. Irshad, R. Nawaz, M.Z. ur Rehman, M. Adrees, M. Rizwan, S. Ali, S. Ahmad, S. Tasleem, Synthesis, characterization and advanced sustainable applications of titanium dioxide nanoparticles: A review, Ecotoxicol. Environ. Saf. 212 (2021) 111978. https://doi.org/10.1016/j.ecoenv.2021.111978.

[34] Muhammad, N. Sofyan, A.H. Yuwono, D. Dhaneswara, A review on green synthesis of

TiO2 nanoparticles: enhancing DSSC performance and exploring future opportunities, Mater. Sci. Energy Technol. 8 (2025) 188–199. https://doi.org/10.1016/j.mset.2025.07.001.

[35] Y. Fu, Y. An, Y. Xu, J.G. Dai, D. Lei, Polymer coating with gradient-dispersed dielectric nanoparticles for enhanced daytime radiative cooling, EcoMat 4 (2022) 1–8. https://doi.org/10.1002/eom2.12169.

[36] X. Song, L. Liu, A.S. Farooq, C.Y. Tso, P. Zhang, Simulated and experimental evaluation of optical property of the polymeric radiative cooling coating with gradient-dispersed particles, Int. J. Therm. Sci. 213 (2025) 109819. https://doi.org/10.1016/j.ijthermalsci.2025.109819.

[37] C.M. Cardinal, Y.D. Jung, K.H. Ahn, L.F. Francis, Drying regime maps for particulate coatings, AIChE J. 56 (2010) 2769–2780. https://doi.org/10.1002/aic.12190.

[38] M. Schulz, J.L. Keddie, A critical and quantitative review of the stratification of particles during the drying of colloidal films, Soft Matter 14 (2018) 6181–6197. https://doi.org/10.1039/c8sm01025k.

[39] Y. Dong, M. Argaiz, B. He, R. Tomovska, T. Sun, I. Martín-Fabiani, Zinc Oxide Superstructures in Colloidal Polymer Nanocomposite Films: Enhanced Antibacterial Activity through Slow Drying, ACS Appl. Polym. Mater. 2 (2020) 626–635. https://doi.org/10.1021/acsapm.9b00991.

[40] J.D. Tinkler, A. Scacchi, M. Argaiz, R. Tomovska, A.J. Archer, H. Willcock, I. Martín-Fabiani, Effect of Particle Interactions on the Assembly of Drying Colloidal Mixtures, Langmuir 38 (2022) 5361–5371. https://doi.org/10.1021/acs.langmuir.1c03144.

[41] C. Sofroniou, A. Scacchi, H. Le, E. Espinosa Rodriguez, F. D'Agosto, M. Lansalot, P.S.M. Dunlop, N.G. Ternan, I. Martín-Fabiani, Tunable Assembly of Photocatalytic Colloidal Coatings for Antibacterial Applications, ACS Appl. Polym. Mater. 6 (2024) 10298–10310. https://doi.org/10.1021/acsapm.4c01436.

[42] M. Anyfantakis, Z. Geng, M. Morel, S. Rudiuk, D. Baigl, Modulation of the coffee-ring effect in particle/surfactant mixtures: The importance of particle-interface interactions, Langmuir 31 (2015) 4113–4120. https://doi.org/10.1021/acs.langmuir.5b00453.

[43] E.D. Eren, M.A. Moradi, H. Friedrich, G. De With, Building Reversible Nanoraspberries, Nano Lett. 21 (2021) 2232–2239. https://doi.org/10.1021/acs.nanolett.0c05059.

[44] Z. Yu, X. Nie, A. Yuksel, J. Lee, Reflectivity of solid and hollow microsphere composites and the effects of uniform and varying diameters, J. Appl. Phys. 128 (2020). https://doi.org/10.1063/5.0015650.

[45] C. Dias, R.C. Veloso, J. Maia, N.M.M. Ramos, J. Ventura, Oversight of radiative properties of coatings pigmented with TiO2 nanoparticles, Energy Build. 271 (2022) 112296. https://doi.org/10.1016/j.enbuild.2022.112296.

[46] J. Song, J. Qin, J. Qu, Z. Song, W. Zhang, X. Xue, Y. Shi, T. Zhang, W. Ji, R. Zhang, H. Zhang, Z. Zhang, X. Wu, The effects of particle size distribution on the optical properties of titanium dioxide rutile pigments and their applications in cool non-white coatings, Sol. Energy Mater. Sol. Cells 130 (2014) 42–50. https://doi.org/10.1016/j.solmat.2014.06.035.

[47] B.Y. Liu, J. Wu, C.H. Xue, Y. Zeng, J. Liang, S. Zhang, M. Liu, C.Q. Ma, Z. Wang, G. Tao, Bioinspired Superhydrophobic All-In-One Coating for Adaptive Thermoregulation,

Adv. Mater. 36 (2024) 1–12. https://doi.org/10.1002/adma.202400745.

[48] A. Muscio, The solar reflectance index as a tool to forecast the heat released to the urban environment: Potentiality and assessment issues, Climate 6 (2018). https://doi.org/10.3390/cli6010012.

[49] Astm G173 − 03, Standard Tables for Reference Solar Spectral Irradiances : Direct Normal and Hemispherical on 37° Tilted Surface, 2020.